IEEE Access
Multidisciplinary | Rapid Review | Open Access Journal

Received 11 March 2023, accepted 18 April 2023, date of publication 26 April 2023, date of current version 3 May 2023.

*Digital Object Identifier 10.1109/ACCESS.2023.3270778*

RESEARCH ARTICLE

# Investigation of AFGSM Methods for Some Electromagnetic Bandgap Structures: From Analysis to Applied Antenna Design

**DURMUS GEBESOGLU[1,3], AGAH OKTAY ERTAY[2], AND SERKAN SIMSEK[3]**

[1]Radar, Electronic Warfare and Intelligence Systems Group, Aselsan Inc., 06200 Ankara, Turkey
[2]Department of Electrical and Electronics Engineering, Faculty of Engineering and Architecture, Erzincan Binali Yildirim University, 24002 Erzincan, Turkey
[3]Department of Electronics and Communication Engineering, Istanbul Technical University (ITU), Maslak, 34469 Istanbul, Turkey

Corresponding author: Durmus Gebesoglu (gebesoglu17@itu.edu.tr)

This work was supported by Aselsan Inc.

**ABSTRACT** Electromagnetic Bandgap (EBG) structures that exhibit various performances, such as preventing the electromagnetic wave propagation and reflecting an incident wave within the stopband, have unique electromagnetic characterization. Due to this reason, accurate analysis and design of the EBG structures are crucial to enhance the integrated system performance. This paper concentrates on the characterization of some planar EBGs using the Auxiliary Functions of Generalized Scattering Matrix (AFGSM) methods, with particular importance on an in-depth consideration of its bandgaps. The AFGSM method is applied to the planar EBG structures in the literature for the first time. The well-known kinds (symmetric and asymmetric cases) of mushroom type and multilayer EBG structures are considered to verify the presented method. Analysis results are compared with the Conventional Eigenvalue Equation (C-EIV) and the Generalized Scattering Matrix based Eigenvalue Equation (GSM-EIV) methods. Low computation load and accurate results are obtained to analyze the planar EBG structures with the AFGSM method due to using transmission line model. In addition, a design methodology is proposed for a chosen planar EBG structure using the AFGSM methods. Geometrical parameters of interested EBG problems are determined for acquiring the stopband frequency region of interest using the scattering parameters of unit cell configuration. The mushroom EBG model along one and two-dimensional axes is used in an antenna application to decrease mutual coupling between antenna elements. Three different scenarios are simulated in the HFSS electromagnetic simulation design environment to understand the effect of mutual coupling reduction in the antenna problem of the designed EBG structure via the AFGSM method. All designed antennas are manufactured, and the measurement results are in good agreement with the simulation results. The measurement results of the fabricated antenna application example including designed EBG using the proposed AFGSM method are compared with the existing similar problems with the same and different EBG models. It has been demonstrated that bandgap analysis, design of the planar EBG structures and integration of considered EBG model to a design application can be accurately and quickly achieved with the given methodology using the AFGSM method.

**INDEX TERMS** Electromagnetic bandgap structures, dispersion diagram, generalized scattering matrix, high impedance surface, periodic structures.

## I. INTRODUCTION

Periodic structures provide passband/stopband frequency characteristics when interacting with electromagnetic waves [1], [2], [3]. Electromagnetic Bandgap (EBG) structures are the periodic structures that possess exciting and unique features via inhibition of electromagnetic wave propagation due to the natural stopband ability to enhance performance characteristics in microwave circuits at certain frequency regions [4], [5], [6]. The EBG structures are utilized in many

The associate editor coordinating the review of this manuscript and approving it for publication was Mahmoud A. Abdalla.

engineering applications such as intensively suppressing of switching noise in high-speed power planes [7], [8], [9], [10], [11], enhancements of microwave filter characteristics [12], [13], [14], improvements of antenna performance [15], [16], [17], [18], low profile antenna design [19], [20], [21], [22], [23], [24] and mutual coupling reduction between antenna elements in antenna arrays [25], [26], [27]. In this context, computation and determination for gathering bandgap information of the EBG structures is an important challenge before using in microwave applications.

There are many bandgap prediction methods [7], [8], [10], [19], [28], [29], [30], [31], [32], [33], [34], [35], [36] in the open literature for analyzing the EBG structures. Lumped element equivalent circuit models are presented in [10], [19], [28], and [29] for estimating the bandgap of some planar EBG structures, such as low-profile antenna applications. In [30] and [31], a transmission line model is proposed for analyzing planar EBG structures. These approximations have an easy way and rapid solutions due to low computational space. However, they include some important assumptions that restrict these techniques' validity. The plane wave expansion method [32] is another technique to gather the bandgap knowledge of the planar EBG structures. Even though this technique is easy to implement, it has some limitations regarding converging the Fourier series and choosing the constituent materials. The computation of band diagrams of the planar EBG structures is based on obtaining classical eigenvalue equations. Two well-known methods called the Conventional Eigenvalue Equation (C-EIV) [7], [30], [31] and the Generalized Scattering Matrix Eigenvalue Equation (GSM-EIV) [33] can be applied to the planar EBG structures to understand the bandgap properties of them. The C-EIV method uses ABCD parameters, whereas the GSM-EIV needs scattering parameters of the unit cell of the planar EBG structures for evaluating their dispersion diagrams. These methods require solving the eigenvalue equation and obtaining network parameters of the EBG structures. Some important studies are proposed for obtaining frequency characterization of the EBG structures based on the Eigenmode method with multiple modes [34], [35], [36]. These efficient techniques need to compute Eigen frequencies of several modes for estimating the band edges of the bandgap regions. Hence, they have a significant computational burden. In [8], an accurate free space method to characterize the frequency behavior of the EBGs using effective electromagnetic parameters is presented. The free space method is used for determining the bandgap regions by i) computing the scattering parameters of the EBG structure with an equivalent circuit model or with full-wave simulation, ii) extracting the effective impedance and refractive index values, iii) finding the complex effective permittivity, and permeability values, iv) obtaining the effective phase and attenuation constants. For this reason, this method includes a long computational step. The Auxiliary Functions of Generalized Scattering Matrix (AFGSM) method, which is firstly described in [33] for symmetrical unit cell assumption of periodic structure and then reformulated for using in an asymmetrical unit cell of periodic structures [37], only needs to the computation of scattering parameters of the unit cell of the periodic structures. This powerful method converts the dispersion problem into a root-finding problem. The AFGSM method can be utilized to find bandgaps of the periodic structures without solving an eigenvalue equation [33], [38], [39]. In this case, a method emerges that can significantly size reduction of the computational effort required for planar electromagnetic bandgap structures. With this theoretical approach straightforwardly explained in [33] and [38], the band edges of the stopband can be accurately calculated by monitoring the zero transitions of auxiliary functions. The AFGSM methods are successfully applied to many periodic structures such as helix slow-wave structures, photonic crystals, dielectric-loaded rectangular waveguides and substrate integrated waveguides [37], [40].

In this paper, we have analyzed the AFGSM methods in the context of planar EBG structures for the first time in the literature. We have demonstrated that these methods can be efficiently used for i) determining the bandgaps of planar EBG structures without solving eigenvalue equations, ii) designing the unit cell parameters of planar EBG structures with the aid of the auxiliary functions and, iii) reducing the mutual coupling between planar antenna elements. In particular, our contributions can be summarized as follows:

- We demonstrate a systematic framework for obtaining unit cell network parameters of the EBG structures, starting from the transmission line circuit model to give a graphical representation of bandgap information of both the conventional and the AFGSM methods in trying to achieve this aim. Four different EBG structures are considered for the applicability and validity of the AFGSM methods. Numerical analysis findings of the AFGSM methods are compared with the C-EIV and GSM-EIV methods. Analysis results of all conventional methods given in this paper for obtaining bandgap properties of the considered EBG structures reveal that the AFGSM methods can be effectively used for the bandgap analysis of EBG structures.
- We evaluated the presented method for designing the EBG structure of the planar antennas to reduce the mutual coupling between antenna elements. The designed EBG structure is periodically loaded as three different scenarios between two antenna elements operating at 3.5 GHz to investigate the possibility of isolation improvement in this antenna problem. Additionally, HFSS simulation results of surface current densities and $|S_{21}|$-dB of designed scenarios of the considered antenna are evaluated for understanding enhancement of isolation using the designed EBG structure with the help of the AFGSM method. Designated antennas are manufactured, and $|S_{21}|$-dB measurements are performed with a vector network analyzer. The performance of manufactured antennas is compared in critical isolation parameters such as total isolation band region, isolation

improvement, and peak isolation concerning specific frequencies and cases. Moreover, the proposed manufactured antenna, including improved isolation performance via the designed EBG model with the AFGSM method, is compared with the open literature involving various EBG models. All these results show that the proposed AFGSM methods give accurate results for the fast and approximate design of the unit cell of the planar EBG structures in a particular microwave application by using scattering parameters information of the 1-D periodic planar EBG model.

## II. EXAMPLES OF SOME EBG STRUCTURES

This section presents transmission line models of some EBG structures, including different geometric configurations available in the open literature [7], [30], [31], [41]. For this purpose, the first planar EBG model includes the asymmetric (off-set via) and symmetric cases of the mushroom-type EBG structure used in decreasing the coupling level between antenna elements in antenna applications. The second planar EBG model involves cases of symmetry and asymmetry of the multilayer EBG model, frequently used for switching noise suppressing in high-speed power planes. Considered EBG structures are given in Fig. 1(a) and 2(a).

### A. EQUIVALENT CIRCUIT MODEL REPRESENTATIONS OF EBG MODELS

This subsection considers circuit model of mushroom-type and multilayer EBG structures given in [7], [19], [30], and [31] to be able to calculate and validate the reported study with standard and AFGSM methods.

#### 1) MUSHROOM EBG STRUCTURE

The unit cell of this problem includes a square metal sheet with shorting post as discussed in [30] and [31]. Periodically loaded electromagnetic bandgap structure shown in Fig. 1(a) can be modeled as reactive loaded resonators, including the effect of gap capacitors. This model [30], [31] involves a half-wavelength microstrip resonator with reactive loading arising from shorting pin. Energy can be propagated along, and above the structure, [30], [31]. Due to this reason, mushroom type EBG structure can be regarded as periodically loaded with gap capacitances and reactance determined by shorting post [30], [31]. Fig. 1(b) demonstrates the equivalent circuit of the mushroom section of the EBG structure. The input impedance of an open-ended transmission line and the impedance after the addition of inductance can be calculated using equations given in [30] and [31]. The microstrip line characteristic impedance is used due to neglectable coupling between adjacent resonators if $(w=(p_1+p_2))/t_1 \geq 2$ where $p_1$, $p_2$ and $t_1$ are left and right length of the metal sheet with the via post and the height of the dielectric substrate, respectively. The characteristic impedance of coplanar waveguide is utilized due to meaningful coupling between adjoint resonators when $(w=(p_1+p_2))/t_1 < 2$ for calculating the input impedance of an open-ended transmission line.

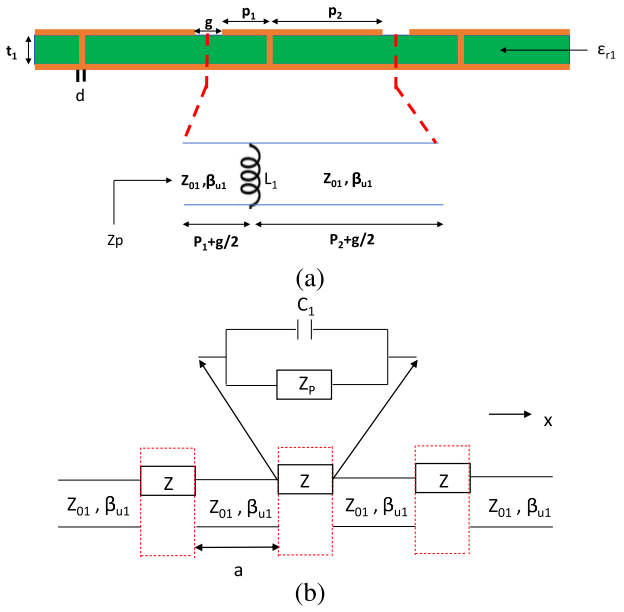


**FIGURE 1.** Considered mushroom-type EBG structure: (a) side view, (b) equivalent circuit of mushroom section of EBG structure.

Characteristic impedance formulas given in [42] are used in our computations. $X_{L_1}$ can be written as $jwL_1$, which is the impedance of the inductance where $w$ and $L_1$ are angular frequency and inductance of the shorting post, respectively. $L_1$ can be found with the following formula [30], [31], [43]:

$$L_1 = 2 \times 10^{-7} t_1 \left[ ln\left(\frac{4t_1}{d}\right) + 0.5\left(\frac{d}{t_1}\right) - 0.75 \right] \quad (1)$$

where d is the diameter of the post. After computing the addition of inductance, the impedance of each resonator section $Z_p$ can be found by using equation 2 shown in [30]. After obtaining the resonator impedance $Z_p$, the coupling capacitor between resonators $X_c$ which is equal to $\frac{1}{jwC_1}$ should be calculated. The capacitance $C_1$ can be obtained using the following formula mentioned in [19], [30], and [31]

$$C_1 = \frac{(p_1 + p_2)\varepsilon_0(1 + \varepsilon_{r1})}{\pi} \cosh^{-1}\left(\frac{(p_1 + p_2 + g)}{g}\right) \quad (2)$$

where $\varepsilon_0$, $\varepsilon_{r1}$ and g are the free space permittivity, dielectric constant of the material and gap between resonators, respectively. Finally, Fig. 1(a) can be acted as a lumped impedance $Z$ formed of $Z_p$ in parallel with $X_c$ with a period of a as shown in Fig. 1(b) which is the 1-D equivalent circuit model of the interested EBG structure. In this context, It is achievable that the frequency characteristic of this EBG structure can be obtained by using the equivalent circuit given in Fig. 1 (b).

#### 2) MULTILAYER EBG STRUCTURE

This EBG structure plays an important role in cutting off wave propagation of Transverse Electric Magnetic (TEM) mode [7]. The multilayer EBG model involves an array of coplanar patch conductors placed a length $t_2$ from the top

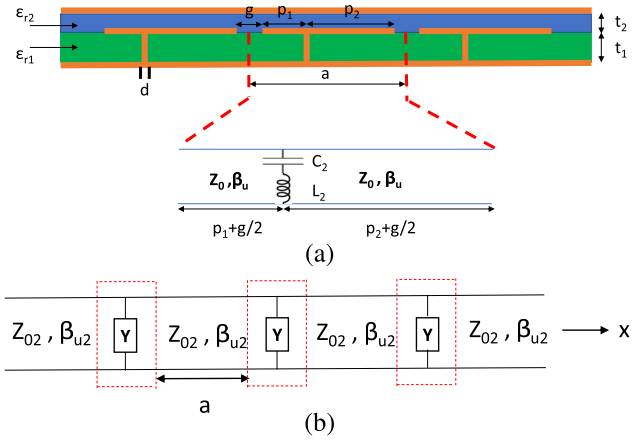


**FIGURE 2.** Considered multilayer EBG structure: (a) side view, (b) equivalent circuit of multilayer section EBG structure.

plate and symmetrical or asymmetrical shorting pins of the length $t_1$ and radius d connecting to the bottom plate of each patch. Square patches and shorting pins are cascaded in a lattice of period a. The patch conductor aims to determine the capacitance between the edge of shorting pin below it and the top plate of the Parallel Plate Waveguide (PPW). In this EBG structure, two dielectric layers are used as the host dielectric medium of the PPW [7]. As mentioned in [7], magnetic walls are used to reduce the 2-D periodic structure to the 1-D array of unit cells to understand the passband and stopband properties of the EBG structure by using an equivalent circuit model. More details about reducing the problem to the 1-D periodic array can be found in [7]. It is well known that the existence of a quasi-TEM model in an empty PPW with magnetic sidewalls can be modeled as a transmission line with the characteristic impedance $Z_0$ and $\beta_u$ given in [7]. A shunt LC circuit can represent conductor patches and shorting pins, as shown in Fig. 2(a). The inductance $L_2$ shown in Fig. 2(b) can be predicted by [7]

$$L_2 = \frac{\mu_0 t_1}{4\pi}[\ln(\frac{1}{\alpha}) + \alpha - 1] \tag{3}$$

where $\mu_0$ and $\alpha$ are the permeability of free space and the ratio of the shorting pin cross-section to the cross-section of the whole unit cell, respectively. The capacitance of this representation for a large diameter of shorting pin can be calculated by [7]

$$C_2 = \frac{\varepsilon_0 \varepsilon_{r_2}((p_1 + p_2)^2 - \frac{\pi d^2}{4})}{t_2}. \tag{4}$$

After calculating $L_2$ and $C_2$, shunt admittance can be given by [7]

$$Y = \frac{j\omega C_2}{1 - \omega^2 L_2 C_2} \tag{5}$$

It is important to note that the shunt admittance is a part of the 1-D equivalent circuit model of the multilayer EBG model, as shown in Fig. 2(a). Hence, it is possible to compute the dispersion diagram of this EBG structure via the circuit model shown in Fig. 2(b). These mentioned equations from (1) to (5) are necessary to obtain network parameters involving in the equivalent circuit models of the considered planar EBG structures.

## III. COMMON BANDGAP PREDICTION METHODS FOR EBG STRUCTURES

This section covers widely used determination methods of bandgap properties of EBG structures.

### A. CONVENTIONAL EIGENVALUE EQUATION METHOD

C-EIV method is based on obtaining network parameters such as ABCD of the unit cell of considered EBG structures.

#### 1) MUSHROOM EBG STRUCTURE

ABCD parameters of the mushroom type EBG structure shown in Fig. 1(a) are given in the following equation:

$$\begin{bmatrix} A & B \\ C & D \end{bmatrix} = \begin{bmatrix} \cos\theta_1 & j\sin\theta_1 \\ j\sin\theta_1 & \cos\theta_1 \end{bmatrix} \times \begin{bmatrix} 1 & \frac{Z}{Z_0} \\ 0 & 1 \end{bmatrix} \times \begin{bmatrix} \cos\theta_2 & j\sin\theta_2 \\ j\sin\theta_2 & \cos\theta_2 \end{bmatrix} \tag{6}$$

where $\theta_1$ and $\theta_2$ are $\beta_{u_1}(p_1+g/2)$ and $\beta_{u_1}(p_2+g/2)$, respectively. When each matrix entry of ABCD parameters in equation 6, A and D can be determined as follows:

$$A = \cos\theta_1\cos\theta_2 + j\frac{Z}{Z_0}\cos\theta_1\sin\theta_2 - \sin\theta_1\sin\theta_2 \tag{7a}$$

$$D = \cos\theta_1\cos\theta_2 + j\frac{Z}{Z_0}\sin\theta_1\cos\theta_2 - \sin\theta_1\sin\theta_2 \tag{7b}$$

The following equation can show the general expression of the eigenvalue equation for periodic structures:

$$\cos(\gamma a) = \begin{cases} \frac{A+D}{2} & A \neq D \\ A & A = D \end{cases} \tag{8}$$

where $\gamma$ indicates complex propagation constant. Eigenvalue equation of the unit cell for given EBG problem can be expressed as $\frac{A+D}{2}$ when the unit cell has no symmetry ($p_1 \neq p_2$) whereas the unit cell has symmetry ($p_1 = p_2$). The considered EBG model is analyzed for the lossless case. Due to this reason, and since the unit cell given in Fig. 1(a) is asymmetric, it is obtained the following equation

$$\cos(\beta a) = \cos(\theta_1 + \theta_2) + j\frac{Z}{2Z_0}\sin(\theta_1 + \theta_2) \tag{9}$$

by arranging equations 7 and 8. When the unit cell of the periodic structure is symmetric, as indicated in [30] and [31], then the C-EIV of the mushroom EBG structure can be written as:

$$\cos(\beta a) = \cos(\beta_u a) + j\frac{Z}{2Z_0}\sin(\beta_u a) \tag{10}$$

where $\beta$ is the propagation constant of the periodic structure. The stopband region of this periodic structure which means an attenuated wave along one-direction can be occurred when

$|\cos(\beta a)| \geq 1$. The passband region can be found when $|\cos(\beta a)| < 1$. Equation (6) can obtain a mushroom EBG structure dispersion diagram.

#### 2) MULTILAYER EBG STRUCTURE

The unit cell of the multilayer EBG structure given in Fig 2(a) can be analyzed by using ABCD parameters as follows [7]:

$$\begin{bmatrix} A & B \\ C & D \end{bmatrix} = \begin{bmatrix} \cos\theta_1 & jZ_0 \sin\theta_1 \\ jY_0 \sin\theta_1 & \cos\theta_1 \end{bmatrix} \times \begin{bmatrix} 1 & 0 \\ Y & 1 \end{bmatrix} \times \begin{bmatrix} \cos\theta_2 & jZ_0 \sin\theta_2 \\ jY_0 \sin\theta_2 & \cos\theta_2 \end{bmatrix}. \quad (11)$$

where $\theta_1$ and $\theta_2$ are $\beta_{u_2}(p_1+g/2)$ and $\beta_{u_2}(p_2+g/2)$, respectively.

$$A = \cos\theta_1 \cos\theta_2 + jYZ_0 \sin\theta_1 \cos\theta_2 - Y_0Z_0 \sin\theta_1 \sin\theta_2 \quad (12a)$$

$$D = \cos\theta_1 \cos\theta_2 + jYZ_0 \cos\theta_1 \sin\theta_2 - Y_0Z_0 \sin\theta_1 \sin\theta_2. \quad (12b)$$

Using general expression of dispersion equation for periodic structure given in equation 8 with assuming lossless case, the following equation can be found:

$$\cos(\beta a) = \cos(\theta_1 + \theta_2) + j\frac{Z_0 Y}{2} \sin(\theta_1 + \theta_2). \quad (13)$$

This equation can be easily used for the asymmetrical case ($p_1 \neq p_2$). When the symmetrical case ($p_1 = p_2$) is considered, the equation 13 can be written as [7]:

$$\cos(\beta a) = \cos(\beta_{u_2} a) + j\frac{Z_0 Y}{2} \sin(\beta_{u_2} a). \quad (14)$$

### B. GENERALIZED SCATTERING MATRIX EIGENVALUE EQUATION METHOD

The main solution point of the GSM-EIV method is to compute scattering parameters of the unit cell of interested EBG models. Figs. 3(a) and 4 (a) demonstrate symmetric ($p_1 = p_2$) / asymmetric ($p_1 \neq p_2$) unit cells of the considered mushroom and multilayer EBG problems, respectively. J1 and J2 depict junctions between impedance $Z$ / admittance $Y$ and transmission line with characteristic impedances $Z_{01}$ /$Z_{02}$ which can be found in [7] and [30] as given in Figs. 1(a) and 2(a). J0 and J3 show the reference planes where scattering parameters of the unit cell are obtained. The scattering parameters of the unit cell of these periodic structures can be expressed as given in matrix form:

$$\begin{bmatrix} b_1 \\ b_2 \end{bmatrix} = \begin{bmatrix} S_{11} & S_{12} \\ S_{21} & S_{22} \end{bmatrix} \begin{bmatrix} a_1 \\ a_2 \end{bmatrix} \quad (15)$$

where $a_{1,2}$ and $b_{1,2}$ are the normalized wave amplitudes of incident and reflected waves from input and output ports [33]. In this problem, the Floquet boundary condition can be imposed due to the 1-D periodicity of the EBG structure, as shown below:

$$\lambda \begin{bmatrix} a_1 \\ b_1 \end{bmatrix} = \begin{bmatrix} b_2 \\ a_2 \end{bmatrix} \quad (16)$$

where $\lambda$ is the complex constant which is specified as $\lambda_{1,2} = e^{\pm j\theta}, \theta = \beta a \in [0, \pi]$. $\beta$ and a are expressed as the Floquet phase factor and the period of the EBG structure, respectively [33]. Equation (17) can be acquired by substituting Equation (16) into Equation (15).

$$\begin{bmatrix} 1 & -S_{11} \\ 0 & -S_{21} \end{bmatrix} \begin{bmatrix} b_1 \\ a_1 \end{bmatrix} + \lambda \begin{bmatrix} -S_{12} & 0 \\ -S_{22} & 1 \end{bmatrix} \begin{bmatrix} b_1 \\ a_1 \end{bmatrix} = 0 \quad (17)$$

Characteristic polynomial equation given in Equation (18) can be obtained by arranging Equation (17) [33].

$$\lambda^2 + \lambda\left[\frac{S_{11}S_{22} - S_{12}S_{21} - 1}{S_{21}}\right] + 1 = 0 \quad (18)$$

Sum of the roots of equation (18) can be written as the following two different forms:

$$\lambda_1 + \lambda_2 = -\left[\frac{S_{11}S_{22} - S_{12}S_{21} - 1}{S_{21}}\right] \quad (19)$$

$$\lambda_1 + \lambda_2 = 2\cos(\beta a) \quad (20)$$

Equating equations (19) and (20), equation (21) can be revealed as follows [33]:

$$cos(\beta a) = \frac{1 - S_{11}S_{22} + S_{12}S_{21}}{2S_{21}}. \quad (21)$$

Equation 21 can be used to analyze the unit cell of the periodic structure, including asymmetrical cases. When the symmetrical and reciprocal cases are taken into account, then the following equation can be obtained [33]:

$$cos(\beta a) = \frac{1 - S_{11}^2 + S_{21}^2}{2S_{21}}. \quad (22)$$

Equations (21) and (22) are alternative forms of Equations (9), (13) and (10), (14) in terms of scattering parameters for asymmetrical and symmetrical cases, respectively. Propagating and non-propagating regions correspond to the passband and stopband of the periodic structure when absolute values of $\cos(\beta a)$ are less and greater equal to unity, respectively. Aforementioned expressions from (6) to (22) is to indicate full detail of achieving eigenvalue equations of planar EBG structures.

## IV. THE PROPOSED AUXILIARY FUNCTIONS OF GENERALIZED SCATTERING MATRIX METHOD FOR EBG STRUCTURES

The theory of the AFGSM method is based on the analysis of stored complex power ($\Psi$) in the unit cell of the periodic structure [33], [39]. It is important to note that the AFGSM method can detect the band edge frequencies by using one of the most crucial advantages of the fact that monitoring zero transitions of $\Psi$ can precisely provide exact positions of bandgap regions [33]. Reference [33] explains more about obtaining complex power stored in the unit cell of the periodic structure. There are two crucial points to understanding the emergence of the AFGSM method. The first point is that real parts of $\Psi$ for the lossless periodic structure must be equal to zero, not only stopband but also passband region. The second point explains that imaginary parts of $\Psi$ must equal

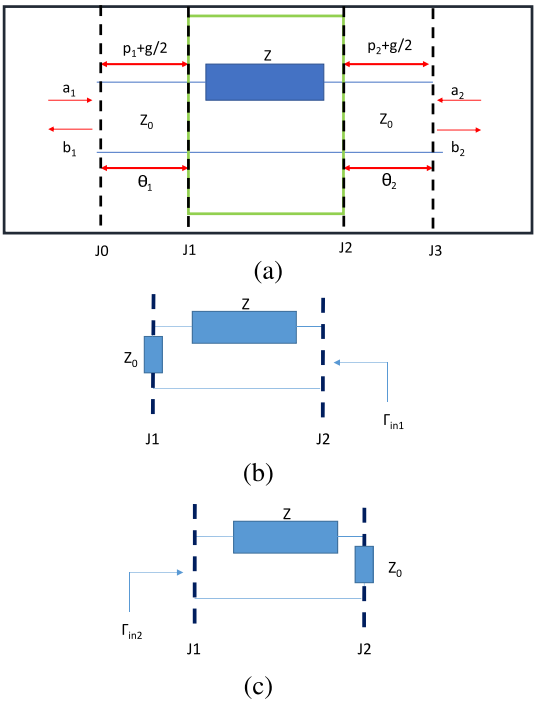


**FIGURE 3.** Unit cell configuration of the mushroom-type EBG structure: (a) asymmetric/symmetric EBG unit cell, (b) matched termination of reference plane J1 of EBG unit cell for obtaining $S_{22}^J$ and $S_{12}^J$, (c) matched termination of reference plane J2 of EBG unit cell for obtaining $S_{11}^J$ and $S_{21}^J$.

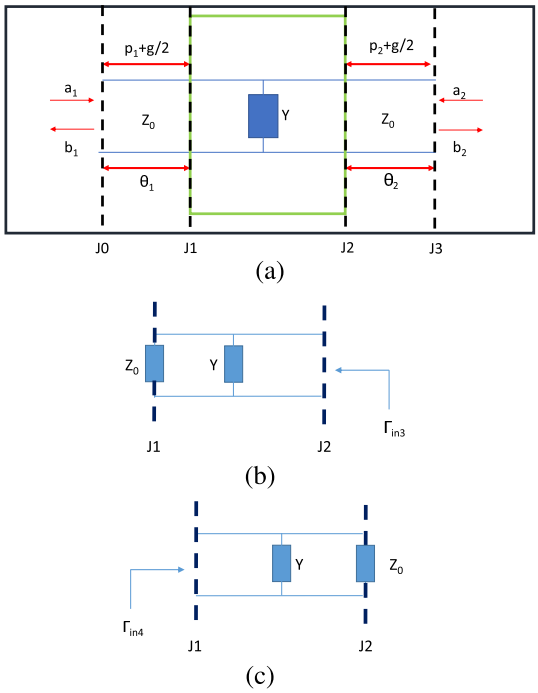


**FIGURE 4.** Unit cell configuration of the multilayer EBG structure (a) asymmetric/symmetric EBG unit cell, (b) matched termination of reference plane J1 of EBG unit cell for obtaining $S_{22}^J$ and $S_{12}^J$, (c) matched termination of reference plane J2 of EBG unit cell for obtaining $S_{11}^J$ and $S_{21}^J$.

zero at the band edge frequencies. A comprehensive AFGSM (C-AFGSM) is derivated in [37] to eliminate the restriction of symmetric unit cell selection of the periodic structure for a single Floquet mode region. The following equation gives an essential solution for determining the band edges of the periodic structure's symmetric/asymmetric unit cell [37].

$$J_1 = 2\,\mathrm{Im}\{S_{11} + 2S_{21}\,\mathrm{Re}\{K_1\} + S_{22}|K_1|^2\} \tag{23a}$$

$$J_{-1} = 2\,\mathrm{Im}\{S_{11} + 2S_{21}\,\mathrm{Re}\{K_{-1}\} + S_{22}|K_{-1}|^2\} \tag{23b}$$

In Equation (23), $K_1$ and $K_{-1}$ equal to $(1 - S_{21})/(S_{22})$ and $(-1 - S_{21})/(S_{22})$, respectively. When a symmetric unit cell is considered in a single Floquet mode region, the following equation can be written as given in [33] and [39]

$$X_{\pm} = \mathrm{Im}\,(S_{11} \pm S_{21}) \tag{24}$$

Zero transitions of the auxiliary functions $J_1$, $J_{-1}$ (C-AFGSM), and $X_+$, $X_-$ (AFGSM) yield the exact values of the band edge frequencies of periodic structures. It is noted that these functions given in equations (23) and (24) are well-behaved functions with frequency, to the best of our knowledge, they have never been used before for obtaining bandgap characterization of the planar EBG structures, and the root-finding procedure can efficiently obtain the zeros of these functions. In this context, The AFGSM methods present an alternative way of finding the band edges of the 1-D EBG structure. The dispersion diagram and behaviors of the auxiliary functions of a 1-D periodic structure can be computed by equations (22) and (23), (24) when the scattering parameters of the unit cell configuration are obtained. Parameters of $S_{11}$ and $S_{21}$, which correspond to the elements of the scattering parameters of the unit cell of the periodic structure, given in equations (22) and (23), (24), can be found by using junction scattering matrices properly and shifting properties of scattering parameters. It is reached at J1 and J2 junctions by taking $\theta_1 = \theta_2 = 0$ to obtain the scattering matrix of the unit cell of the periodic structure given in Figs. 3(a) and 4(a). After then, it is necessary to attain the scattering parameters regarding the J1 junction demonstrated in Figs. 3(b) and 4(b). For this purpose, the junction scattering parameters, $S_{22}^J$, $S_{12}^J$, are acquired by matching termination of junction J1, utilizing the continuity of voltage at the junction and using reflection coefficients $\Gamma_{in1}$ in Fig. 3 (b) and $\Gamma_{in3}$ in Fig. 4(b). The same manner is applied to the junction of J2 by using reflection coefficients $\Gamma_{in2}$ and $\Gamma_{in4}$ in Figs. 3(c) and 4(c), the junction scattering parameters of J2, $S_{11}^J$, $S_{21}^J$ are obtained. After calculating the scattering parameters at the junctions, the scattering parameters of the 1-D periodic structure ($S_{11}$, $S_{12}$, $S_{21}$, $S_{22}$) can be evaluated by shifting reference planes J1 and J2.

## V. NUMERICAL ANALYSIS AND DESIGN RESULTS

This part involves testing and controlling the analysis of the conventional and the AFGSM methods and design and

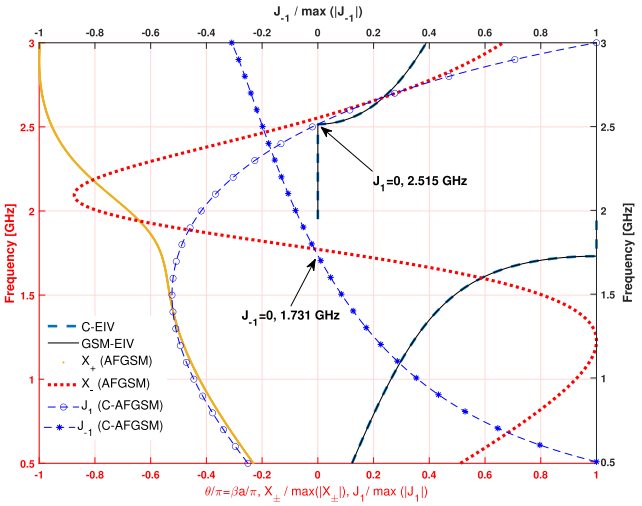


**FIGURE 5.** Frequency responses of the C-EIV, GSM-EIV and AFGSM methods for asymmetric case of Fig. 1(a) with dimensions a = 18 mm, $p_1$ =6 mm, $p_2$ =10 mm, g = 2 mm, $t_1$ = 4 mm, d = 0.5 mm and $\varepsilon_r$ = 2.2 given in [41].

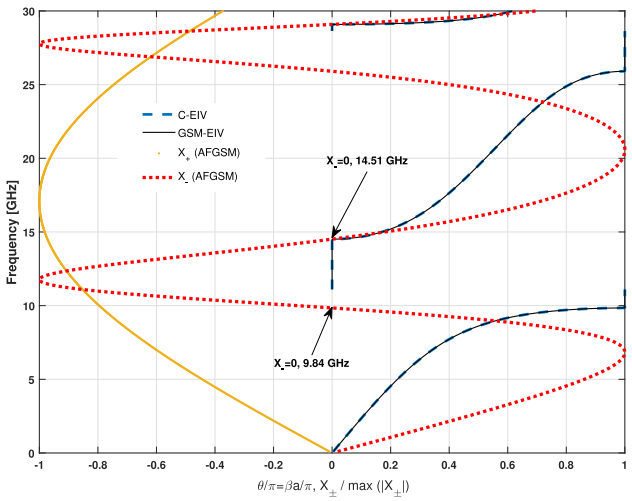


**FIGURE 6.** Frequency responses of the C-EIV, GSM-EIV and AFGSM methods for symmetric case of Fig. 1(a) with dimensions a =3.25 mm, $p_1$ = 1.5 mm, $p_2$ = 1.5 mm, g =0.25 mm, $t_1$ = 1.5 mm, d = 0.5 mm and $\varepsilon_r$ = 2.2 given in [30].

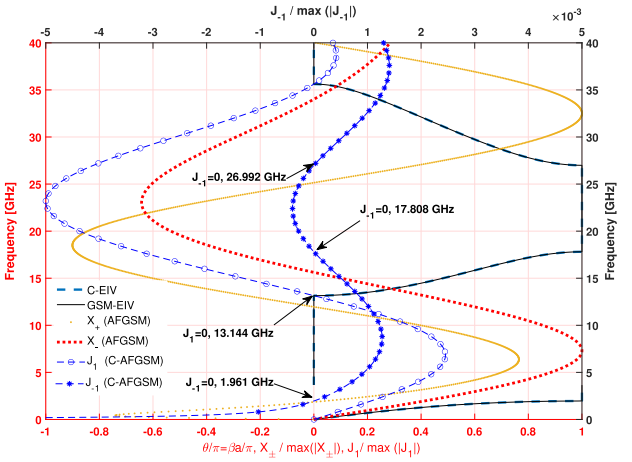


**FIGURE 7.** Frequency responses of the C-EIV, GSM-EIV and AFGSM methods for asymmetric case of Fig. 2(a) with dimensions a = 5.59 mm, $p_1$ = 3 mm, $p_2$ = 2.08 mm, g = 0.51 mm, $t_1$ = 0.79 mm, $t_2$ = 0.051 mm d = 0.5 mm, $\varepsilon_{r1}$ = 2.2, $\varepsilon_{r2}$ = 4.5.

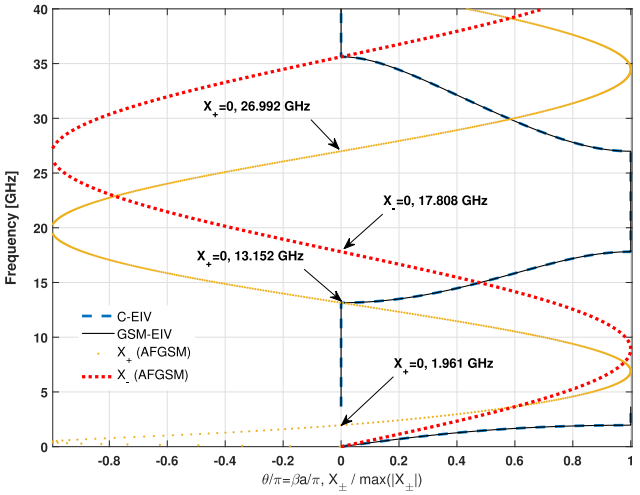


**FIGURE 8.** Frequency responses of the C-EIV, GSM-EIV and AFGSM methods for symmetric case of Fig. 2(a) with dimensions a = 5.59 mm, $p_1$ = 2.54 mm, $p_2$ = 2.54 mm, g = 0.51 mm, $t_1$ = 0.79 mm, $t_2$ = 0.051 mm d = 0.5 mm, $\varepsilon_{r1}$ = 2.2, $\varepsilon_{r2}$ = 4.5 given in [7].

implementation stages using the proposed AFGSM method for planar EBG structures in the previous sections.

### A. ANALYSIS OF PASSBAND/STOPBAND REGIONS

Considered EBG structures given in Fig. 1(a) and Fig. 2(a) can be solved analytically and compared with the numerical results in [7] and [30]. In this study, the same EBG structures are analyzed by solving C-EIV methods given in equations (10) and (14). In addition to this solution, starting from the equivalent circuit representation of the considered EBG structure, an eigenvalue equation is obtained based on the GSM solution (GSM-EIV). The third method (AFGSM) for obtaining the passband/stopband region of interested EBG structures is also procured in this work. Figs. 5, 6, 7 and 8 illustrate the solutions of the considered EBG structures given in section II of the C-EIV methods given in (10) and (14), the GSM-EIV method given in (21) and the proposed AFGSM method solutions for the structure given in Figs. 1(a) and 2(a). All analysis parameters are given in captions of Figs. 5, 6, 7 and 8. Results are perfectly matched for the EIV (C-EIV and GSM-EIV) solutions. Figs. 5 and 6 demonstrate the results of conventional EIV and the proposed AFGSM methods for an asymmetric and a symmetric unit cell model of mushroom-type EBG structure, respectively. It can be seen that the $X_+$ and $X_-$ functions derived from the symmetric unit cell assumption try to find the band edges with a certain error as shown in Fig. 5. Moreover, $J_1$ and $J_{-1}$ functions can determine the band edges exactly. AFGSM functions can detect band edges exactly for symmetric unit cell configuration as

shown in Fig. 6. Figs. 7 and 8 illustrate dispersion diagrams of C-EIV, GSM-EIV and the results of the proposed AFGSM methods for an asymmetric and a symmetric unit cell model of multilayer EBG structure, respectively. It can be revealed here that the AFGSM and C-AFGSM methods can successfully determine band edges of symmetric unit cell configuration of the multilayer EBG structure. In contrast, only the CAFGSM functions can accurately detect passband/stopband boundary frequencies for asymmetric unit cell configuration. $\theta$ is equal to $\pi$ at the beginning of the stopband, on the other hand, $\theta$ equals 0 at the end of the stopband observed in Fig. 5. The function of $J_{-1}$ can exactly find the band edge where $\theta$ is equal to $\pi$. The band edge where $\theta$ equals 0 can be precisely determined by monitoring the function of $J_1$. This mathematical result is because the derived functions $J_{-1}$ and $J_1$ are obtained by forcing $\lambda = e^{j\pi}$ and $\lambda = e^{j0}$, respectively, in the expression of the complex power stored in the unit cell of the periodic structure. It is important to note that just one auxiliary function tries to find the band edges frequencies where $\theta$ can have different values for one stopband region in a symmetric unit cell configuration as shown in Figs. 6 and 8. Functions of $X_+$ and $X_-$ can predict the band edges of the periodic structure together for a stopband region where $\theta$ is equal to the same value ($\theta = 0$ or $\theta = \pi$ along the whole stopband region). It is expected result that the functions of $X_+$ and $X_-$ can estimate the band edge frequencies of the periodic structure either separately or together due to the existence of $|S_{11}| = |1 \pm S_{21}|$ at the band edge frequencies. It can be seen from Figs. 5, 6, 7 and 8 that the band edge results for the CAFGSM method are in good agreement with the other two methods. The C-EIV and GSM-EIV methods are based on the knowledge of the computation of ABCD and scattering parameters of the EBG unit cell. The critical point for the AFGSM method is to compute the scattering parameters of the considered EBG structures. This case can be performed via an equivalent circuit model of the EBGs or using different electromagnetic design environments. After obtaining the scattering parameters of the EBG unit cell, finding the band edges with the root finding routine using the functions in the AFGSM methods present a mathematically simple solution compared to other methods. This shows that the proposed methods can make a more effective and easy analysis. It is important to say that the AFGSM methods can be effectively used as an alternative way of obtaining passband/stopband regions of the planar EBG structure. These results can open the door to designing EBG structures for specific applications.

### B. APPLICATION TO ANTENNA PROBLEM OF DESIGNED EBG VIA AFGSM METHOD

The previous section has effectively discussed the success of AFGSM methods in determining the passband/stopband regions of planar EBG structures. The AFGSM method can also be tested to determine the design parameters of planar EBG structures for a specific purpose. For this purpose, this section establishes an application procedure for reducing the mutual coupling effects with an appropriate planar EBG model to be designed by the AFGSM method in antenna array applications. A rectangular patch array antenna example is designed as shown in Fig. 9(a). Considered operation frequency (3.5 GHz) of this antenna design application can

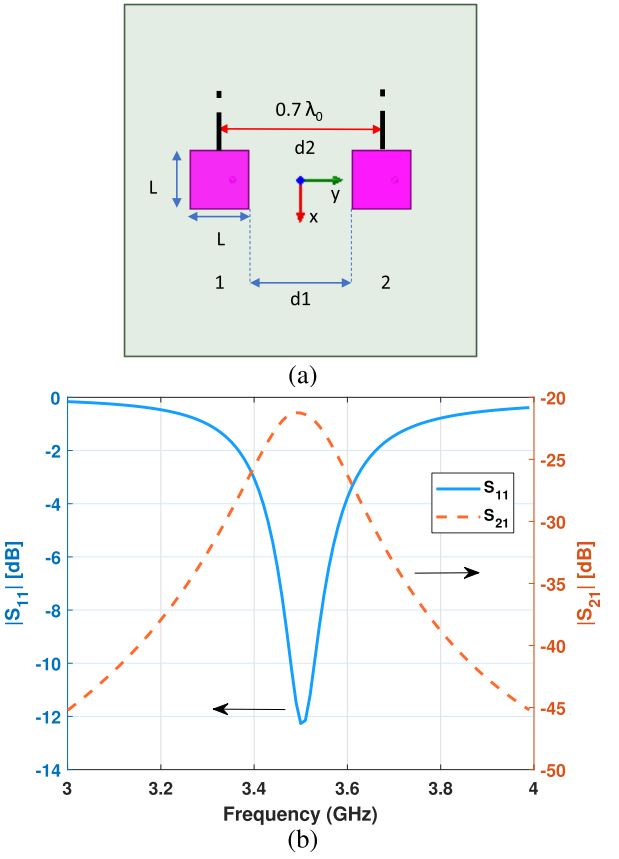


**FIGURE 9.** Considered antenna scenario with (a) top view and (b) simulation results of $|S_{11}|$-dB and $|S_{21}|$-dB frequency responses.

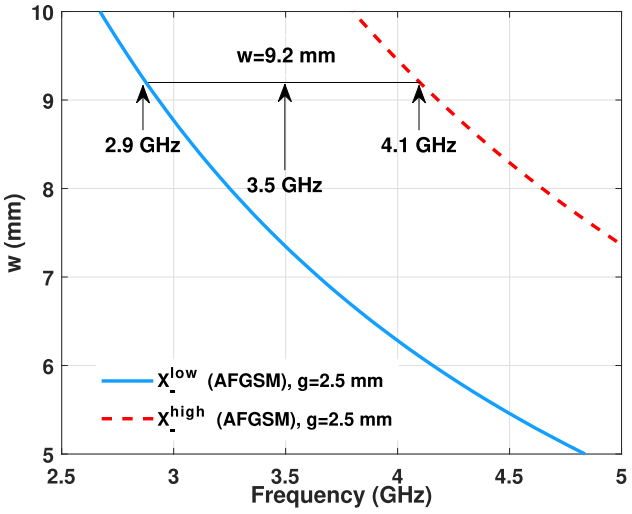


**FIGURE 10.** Design curves of (w,g) pairs for choosing proper bandgap information.

be suitable for Fifth Generation (5G) communication systems. The top view, parametric details, and $|S_{11}|$ frequency characteristic of the coaxial line fed two-element microstrip patch antenna array are given In Fig. 9. This application procedure is tested using Rogers 4003 material with $\varepsilon_r = 3.55$, and h=1.524 mm. As is seen in Fig. 9 (b), the antenna has an operating frequency of 3.5 GHz and a bandwidth of approximately 50 MHz. It can be seen from Fig. 9(b) that the isolation levels between antenna elements are at -21 dB levels near the operation frequency. Although it seems an excellent option to increase the distance between the antenna elements to reduce the mutual coupling, it is seen that circuit size can be increased in this case. For this reason, it is aimed to model suitable planar EBG structures and apply them to this problem with nearly the same magnitude of $S_{11}$ frequency characteristic of the existing antenna arrays with the same circuit dimensions. Accordingly, EBG design dimensions are determined by the AFGSM method. The mushroom-type EBG structure is chosen as the test model. In this model, the parameters w and g majorly affect the passband/ stopband characteristics. The band edges of stopbands formed by setting free the w and g parameters of the mushroom type EBG structure in specific value ranges can be determined by the AFGSM method. Each curve is created by recording the band edge frequencies formed by sweeping the w parameter against a g value. To effectively reduce the $|S_{21}|$ level in the frequency range of operation, w and g values, ensure that the center frequency of the EBG structure is such that the center frequency of the stopband comes to 3.5 GHz, can be found using the design curves in Fig. 10. For any (w, g) pair, detection of stopband can be made by the frequency difference between the design curves ($X_{-}^{low}$ and $X_{-}^{high}$) that find the corresponding band edges. In Fig. 10, when a horizontal line is drawn for the fixed value of w, the $X_{-}^{low}$ and $X_{-}^{high}$ values that cross the line indicate the band edge frequencies of the stopband region ($X_{-}^{low}$=0, at 2.9 GHz and $X_{-}^{high}$=0, at 4.1 GHz). Since the center frequency of the stopband is desired to be 3.5 GHz, the corresponding w and g values are found as 9.2 mm and 2.5 mm from Fig. 10, respectively. After this determination is made, a suitable EBG unit cell design is obtained. From this point on, the planar EBG model, whose design dimensions are determined by the AFGSM method, can be applied to the two-element antenna array problem. To see the effect of the designed EBG model on the antenna problem, the designed EBG model was placed between the antenna elements, first with 1 × 3 elements and then with 3 × 3 and 9 × 3 elements, respectively. In Fig. 11, surface current distributions are given in the antenna application operating at 3.5 GHz, when there is no EBG, and various EBG arrays are present. The distance between the antennas is preserved in the considered scenario. Current distributions in both antennas are observed by excitation of Antenna 1. When there is no EBG between antenna elements, it is seen from the current distribution values that the mutual coupling has a strong effect in Fig. 11(a). It can be clearly said from Fig. 11(b), (c), and (d) that the increase in size and number of EBG arrays can significantly reduce the coupling effects between the two antennas.

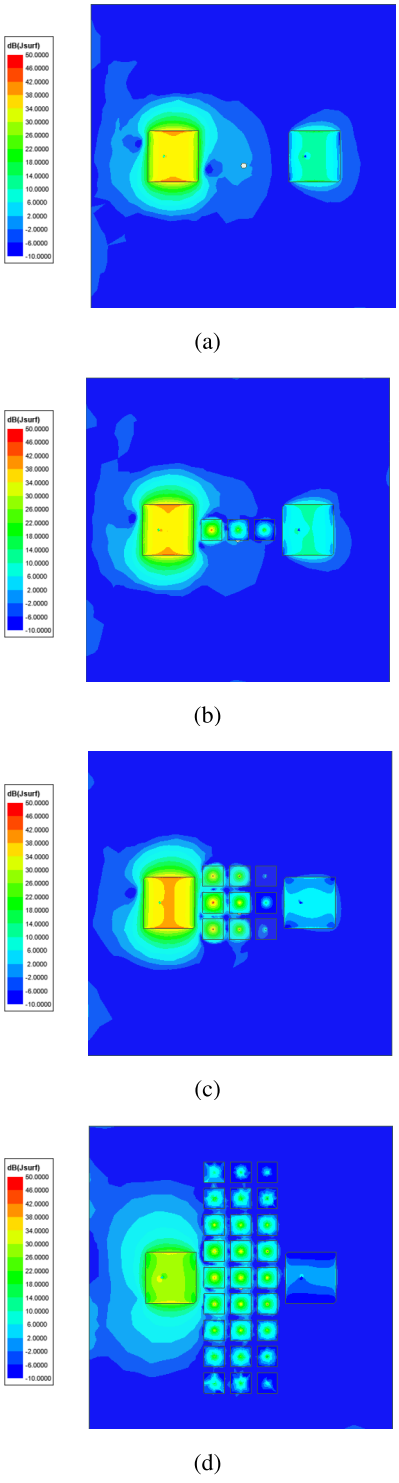


**FIGURE 11.** Surface current distribution of considered antenna scenarios (a) with no EBG (b) with 1 × 3 EBGs (c) with 3 × 3 EBGs (d) with 9 × 3 EBGs at 3.5 GHz.

It can be stated from Fig. 11(b), (c), and (d) that the lowest mutual coupling occurs when there is a 9 × 3 EBG elements

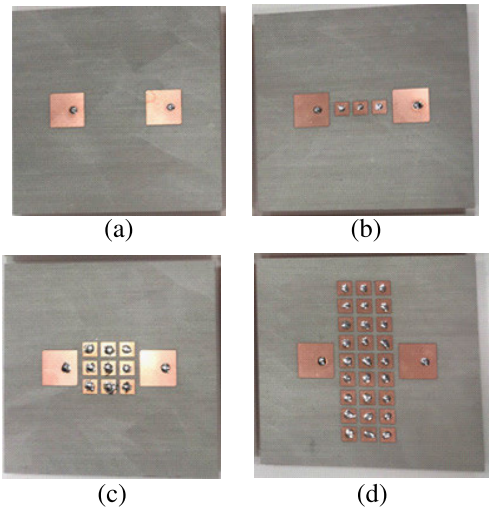


**FIGURE 12.** Top views of manufactured antennas (a) with no EBG (b) With 1 × 3 EBGs (c) with 3 × 3 EBGs (d) with 9 × 3 EBGs.

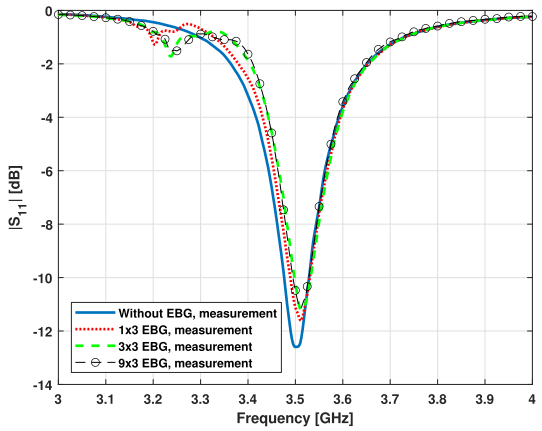


**FIGURE 13.** Measurement results of $|S_{11}|$-dB frequency responses for manufactured antennas.

between the two antennas. The antenna model of each scenario is manufactured to carry out the critical measurement stages, and these antennas are given in Fig. 12. Fig. 13 demonstrates $|S_{11}|$-dB frequency characteristics of manufactured antennas. As expected, applying the EBG structures to the proposed antenna does not have significant effects on the antenna's $|S_{11}|$-dB performance because these EBGs significantly improve the antenna's isolation performance. It is seen in Fig. 14 that the simulation and measurement results have consistent results. It is seen in Fig. 14(b), (c), and (d) that there are slight discrepancies between the measurement and simulation results, especially in the frequency region of operation. The simulation and measurement results of $|S_{21}|$ frequency characteristics showing the measure of coupling between antenna elements belonging to different scenarios are given in Fig. 14. It is thought that this difference may be caused by the difficulties experienced in the manufacturing process due to the sensitive values of the shorting post diameters in the EBG models. Fig. 14 shows a strong mutual

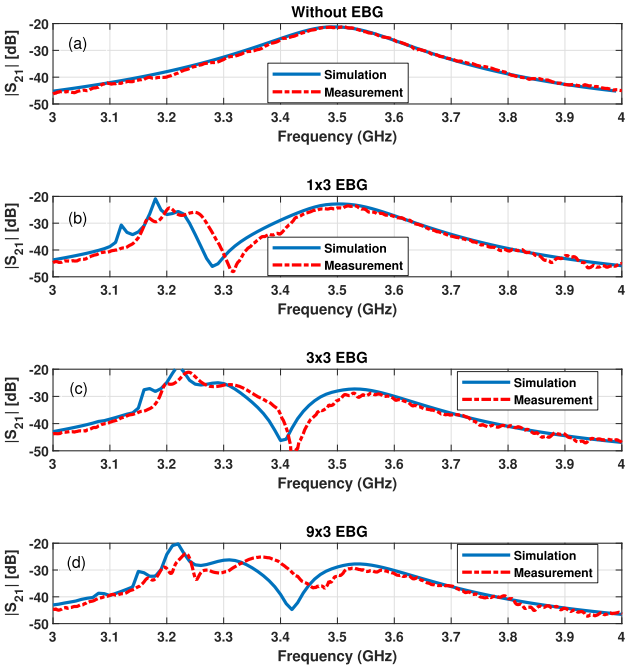


**FIGURE 14.** Simulation and measurement results of $|S_{21}|$-dB frequency responses for designated scenarios.

coupling level with -21 dB in the absence of EBG between antenna elements at 3.5 GHz. It is observed in Fig. 14 that the mutual coupling at 3.5 GHz decreased by 2 dB and 14 dB by using 1 × 3, 3 × 3, and 9 × 3 EBG arrays, respectively. It is seen that the $|S_{21}|$ levels decrease significantly in the operating frequency region of the antenna for the scenario with the 9 × 3 EBG model. Figs. 15 and 16 depict the 2D co-polarization and cross-polarization radiation patterns of the proposed antennas for $\phi = 0°$ and $\phi = 90°$ at 3.5 GHz. As shown in Figs. 15 and 16, there is no significant change between those without EBG and with different EBG cases for co-polarization radiation patterns. Adding EBGs between antennas increases cross-polarization radiation patterns slightly for $\phi = 0°$. The values of the cross-polarization radiation pattern may be reduced for $\phi = 90°$ when increasing the number of EBGs, as demonstrated in Fig. 16. It is evident that total efficiencies are stable and greater than 80% around an operation frequency of 3.5 GHz, as shown in Fig. 17. One clearly says that adding EBG structures between antenna elements gives rise to frequency shifting and a reduction in total efficiency up to 3.52 GHz. $|S_{11}|$ and $|S_{21}|$ are related to mismatching and coupling losses for the total efficiency calculation of two port antennas, respectively. The total efficiency of the Antenna 1 is proportional to the $(1 - |S_{11}|^2 - |S_{21}|^2)$ [44], [45]. As it is seen from Fig. 13 and Fig. 14, $|S_{11}|$ (dB) values are considerably greater than $|S_{21}|$ (dB) values. $|S_{11}|$ (dB) values significantly affect the total efficiency than $|S_{21}|$ (dB) values. Therefore, it can be expressed that the total efficiencies of the antennas with resonance behavior first increase then decrease since the variation of $|S_{11}|$ behaves as decreasing to the resonant frequency

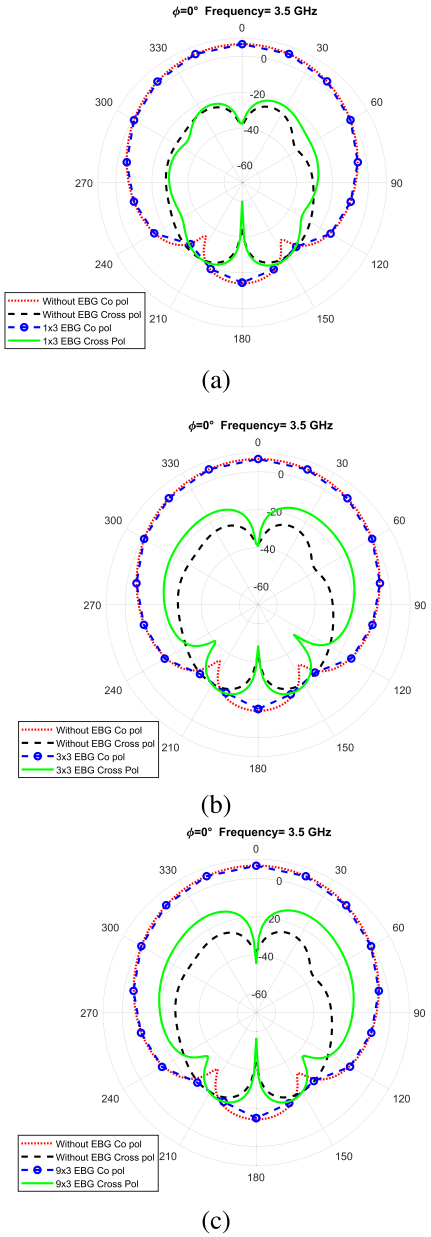


**FIGURE 15.** Simulated $\phi = 0°$ co and cross polarization radiation patterns of proposed antennas for comparing (a) without EBG and 1 × 3 EBG (b) without EBG and 3 × 3 EBG (c) without EBG and 9 × 3 EBG on $\theta$ plane at 3.5 GHz.

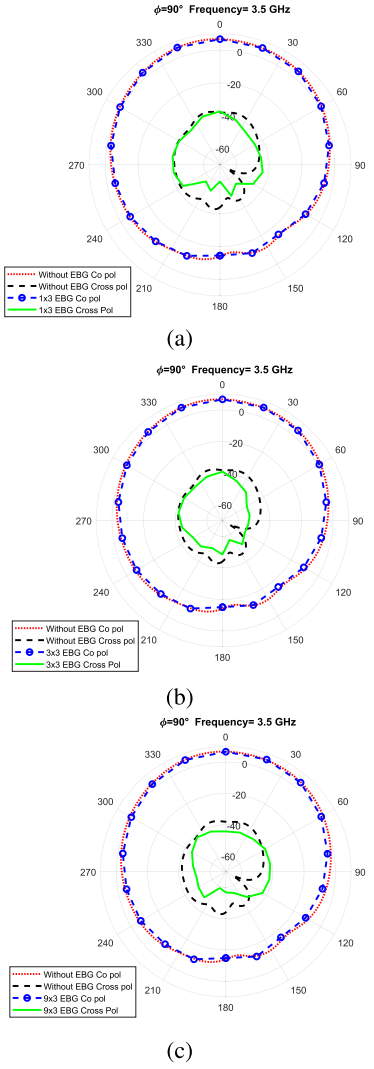


**FIGURE 16.** Simulated $\phi = 90°$, co and cross polarization radiation patterns of proposed antennas for comparing (a) without EBG and 1 × 3 EBG (b) without EBG and 3 × 3 EBG (c) without EBG and 9 × 3 EBG on $\theta$ plane at 3.5 GHz.

and increasing after the resonant frequency. Fig. 18 shows proposed antennas' Envelope Correlation Coefficient (ECC) performance based on radiation patterns [46], [47], [48]. It is clearly seen that the designed EBG unit cell with the AFGSM method provides an important effect in improving the ECC performance of the proposed antenna. When the EBG structure designed in appropriate dimensions is arranged from one to two dimensions, the ECC values become very close to zero in the operating frequency range.

Table 1 shows the effects of applying designed EBG structures via the AFGSM method with a proper arrangement for a patch array antenna application by highlighting their improvements in mutual coupling reduction. The comparison is made to several performance parameters related to

**TABLE 1.** Performance comparisons of the proposed antennas.

| Scenarios | TIBR (MHz) [a] | II (dB) [b] at 3.5 GHz | II (dB) [c] at 3.42 GHz | PI (dB) [d] |
|---|---|---|---|---|
| I. With no EBG | 200 | - | - | -33.4 near to 3.3 GHz |
| II. With 1 × 3 EBG | 220 | 3 | 7.5 | -48.1 near to 3.31 GHz |
| III. With 3 × 3 EBG | 260 | 10 | 35.6 | -57.1 near to 3.42 GHz |
| IV. With 9 × 3 EBG | 330 | 11 | 9.8 | -36.85 near to 3.48 GHz |

[a] Total isolation band region with respect to -30 dB between 3.2 - 3.7 GHz.
[b] Isolation improvement with respect to the Scenario I.
[c] Isolation improvement with respect to the Scenario I.
[d] Peak isolation between 3.2 - 3.7 GHz

**TABLE 2. Performance comparisons of the proposed antenna with respect to similar previous works.**

| Studies | $f_0$* (GHz) | $\varepsilon_{r1}$ | $\varepsilon_{r2}$ | $t_1$ (mm) | $t_2$ (mm) | Edge-to-Edge Distance (mm) | Enhancement in $\lvert S_{21}\rvert$ at $f_0$ (dB) | EBG dimensions (mm × mm) | Number of EBGs | g (mm) |
|---|---|---|---|---|---|---|---|---|---|---|
| [25], Fig. 16 | 5.86 | 10.2 | - | 1.95 | - | 38.8 | 7.8 | 3 × 3 | 56 | 0.5 |
| [26], Fig. 17 | 3.06 | 10 | 1 | 2.54 | 6 | 45 | 15 | 22 × 15 | 4 | 7 |
| [49] Fig. 7 | 5.81 | 9.8 | - | 2 | - | 43 | 10 | 6.2 × 6.2 | 21 | 0.8 |
| [50], Fig. 11 | 5.6 | 4.4 | - | 1.5 | - | 53.57 | 9 | 15 × 15 | 12 | not given |
| [51], Fig. 6 | 2.45 | 4.3 | - | 2 | - | 22 | 8.13 | 6.44 × 6.44 | 24 | 0.2 |
| This study, Scenario IV. | 3.51 | 3.55 | - | 1.524 | - | 38.27 | 10 | 9.2 × 9.2 | 27 | 2.5 |

* This frequency is based on the measurement results.

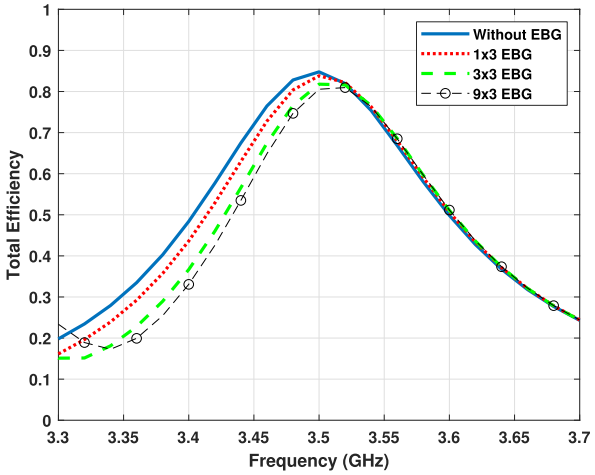


**FIGURE 17. Total efficiencies of proposed antennas.**

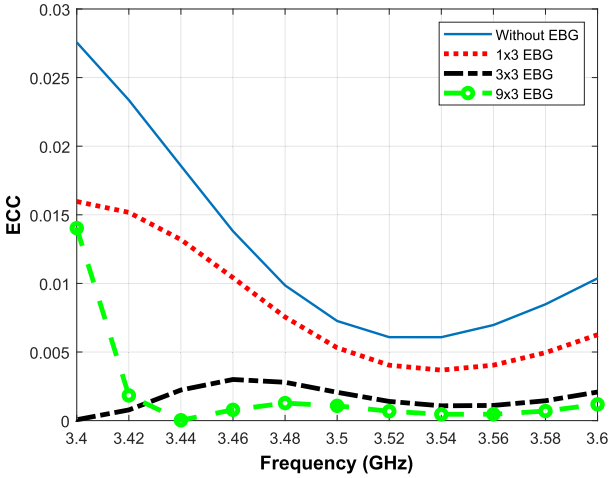


**FIGURE 18. The ECC results of proposed antennas based on radiation patterns.**

isolation, such as total isolation bandwidth, isolation improvement, and peak isolation. One can observe from Table 1 that the considered antenna with 9 × 3 EBGs has better total isolation bandwidth concerning −30 dB for the frequency region of interest. It can be seen that high isolation is performed for the considered antenna with 9 × 3 EBGs at 3.5 GHz. It can be seen from Table 1 that increasing the number of EBGs between antennas and periodic arrangement in two dimensions have a significant impact on reducing the mutual coupling level.

Table 2 depicts performance comparisons of the final antenna with the designed EBG model via the proposed AFGSM method. Mutual properties of given open literature [25], [26], [49] are to have similar patch antenna array geometry and include mushroom type, multilayer EBG structures. The measurement results of all studies are considered in Table 2. It is significant to emphasize that [25] has a minimum enhancement for mutual coupling reduction even if it has much more EBGs than other works given in Table 2. Another point is that maximum enhancement for isolation is obtained in [26] due to using EBG without via in multilayer substrate with low and high dielectric permittivity. This case can reduce the edge-to-edge distance of the antenna elements. However, using an antenna application with a multilayer substrate has a circuit complexity to [25] and [49] and this work. Moreover, as a result of approximately determining the unit cell dimensions of the EBG from the circuit model and integrating it into the antenna problem in the electromagnetic simulation environment, a moderate isolation improvement is achieved between the antenna elements. To obtain higher levels of isolation improvements, precise EBG unit cell design with the proposed AFGSM method and applying it to the antenna problem in full-wave simulation programs will yield effective results. It can be clearly said that the designed EBG model with the proposed AFGSM method has a stronger impact on reducing the mutual coupling between rectangular patch antenna elements about different EBG structure performances given in [50] and [51]. Another point is that reducing the mutual coupling between antennas presents a significant challenge, especially in Multiple-Input Multiple-Output (MIMO) antennas. In addition to EBG structures, novel and powerful mutual coupling reduction methods have become vital in the open literature [47], [48]. Unlike EBG structures, Decoupling and matching circuits used in [47] and [48] to

increase isolation between antenna elements affect antenna performance significantly rather than EBG structures.

## VI. CONCLUSION

This paper has investigated the applicability of the AFGSM method to the detection of passband/stopband regions of planar electromagnetic bandgap structures. The bandgap properties of some planar EBG structures with asymmetric and symmetric unit cell properties are determined by the AFGSM method. The results are confirmed by the methods available in the literature. After obtaining consistent results, the approximate determination of the unit cell design of planar EBG structures is made by the AFGSM method. The solution of reducing the mutual coupling effects between the antennas with the designed EBG structure and its success in this problem are discussed. As a result, it has been seen that the AFGSM methods can be efficiently applied in the analysis and design of planar EBG structures. Furthermore, the presented AFGSM method can be used for complex planar EBG structures to obtain accurate estimation of bandgap edge frequencies when scattering matrix elements of 2-D periodic planar EBG structures are determined by analytical, semi-analytical approaches or simulations in full-wave electromagnetic design environments. Two critical problems are planned to be addressed as a further study. First, examining the success of the AFGSM methods in scenarios involving different types of symmetry found in the unit cell of planar EBG structures [12], [52], [53] can be exciting research. Finally, it is possible to determine the passband/stopband regions in such structures by using the scattering parameter information of the unit cell of periodic planar EBG structures in two dimensions [11] with a new AFGSM approach.

## ACKNOWLEDGMENT

The authors would like to thank Aselsan Inc. for the support provided electromagnetic simulation environment, manufacturing and measurement of the antennas.

## CONFLICT OF INTEREST

The authors declare no potential conflict of interests.

## REFERENCES

[1] R. E. Collin, *Field Theory of Guided Waves*. Hoboken, NJ, USA: Wiley, 1990.
[2] A. A. Tavallaee, "On the stopband characterization of periodic structures," Ph.D. thesis, Dept. Elect. Comput. Eng., McGill Univ., Montreal, QC, Canada, 2006.
[3] F. Yang and Y. Rahmat-Sami, *Electromagnetic Band Gap Structures in Antenna Engineering*. Cambridge, U.K.: Cambridge Univ. Press, 2009.
[4] O. Sokunbi and H. Attia, "Highly reduced mutual coupling between wideband patch antenna array using multiresonance EBG structure and defective ground surface," *Microw. Opt. Technol. Lett.*, vol. 62, no. 4, pp. 1628–1637, Apr. 2020.
[5] P. Samineni, T. Khan, and A. De, "Modeling of electromagnetic band gap structures: A review," *Int. J. RF Microw. Comput.-Aided Eng.*, vol. 27, no. 2, Feb. 2017, Art. no. e21055.
[6] M. Bozzi, S. Germani, L. Minelli, L. Perregrini, and P. de Maagt, "Efficient calculation of the dispersion diagram of planar electromagnetic band-gap structures by the MoM/BI-RME method," *IEEE Trans. Antennas Propag.*, vol. 53, no. 1, pp. 29–35, Jan. 2005.
[7] S. D. Rogers, "Electromagnetic-bandgap layers for broad-band suppression of TEM modes in power planes," *IEEE Trans. Microw. Theory Techn.*, vol. 53, no. 8, pp. 2495–2505, Aug. 2005.
[8] Y. T. Aladadi and M. A. S. Alkanhal, "Accurate characterization of electromagnetic band-gap structures," *IEEE Access*, vol. 9, pp. 121654–121664, 2021.
[9] T. Kamgaing and O. M. Ramahi, "Design and modeling of high-impedance electromagnetic surfaces for switching noise suppression in power planes," *IEEE Trans. Electromagn. Compat.*, vol. 47, no. 3, pp. 479–489, Aug. 2005.
[10] S. Shahparnia and O. M. Ramahi, "A simple and effective model for electromagnetic bandgap structures embedded in printed circuit boards," *IEEE Microw. Wireless Compon. Lett.*, vol. 15, no. 10, pp. 621–623, Oct. 2005.
[11] Y. Toyota, A. E. Engin, T. H. Kim, and M. Swaminathan, "Stopband analysis using dispersion diagram for two-dimensional electromagnetic bandgap structures in printed circuit boards," *IEEE Microw. Wireless Compon. Lett.*, vol. 16, no. 12, pp. 645–647, Dec. 2006.
[12] B. A. Mouris, A. Fernandez-Prieto, R. Thobaben, J. Martel, F. Mesa, and O. Quevedo-Teruel, "On the increment of the bandwidth of mushroom-type EBG structures with glide symmetry," *IEEE Trans. Microw. Theory Techn.*, vol. 68, no. 4, pp. 1365–1375, Apr. 2020.
[13] J. Lim, S. Oh, S. Lee, W. Yoon, and J. Lee, "Enhanced broadband common-mode filter based on periodic electromagnetic bandgap structures," *Microw. Opt. Technol. Lett.*, vol. 60, no. 12, pp. 2932–2937, Dec. 2018.
[14] J. A. Brown, S. Barth, B. P. Smyth, and A. K. Iyer, "Compact mechanically tunable microstrip bandstop filter with constant absolute bandwidth using an embedded metamaterial-based EBG," *IEEE Trans. Microw. Theory Techn.*, vol. 68, no. 10, pp. 4369–4380, Oct. 2020.
[15] S. Jam and M. Simruni, "Performance enhancement of a compact wide-band patch antenna array using EBG structures," *AEU-Int. J. Electron. Commun.*, vol. 89, pp. 42–55, May 2018.
[16] J.-Y. Lee, J. Choi, J.-H. Jang, and W. Hong, "Performance enhancement in compact inverted-L antenna by using 1-D EBG ground structures and beam directors," *IEEE Access*, vol. 7, pp. 93264–93274, 2019.
[17] M. K. Abdulhameed, M. S. B. M. Isa, Z. Zakaria, I. M. Ibrahim, M. K. Mohsen, M. L. Attiah, and A. M. Dinar, "Radiation control of microstrip patch antenna by using electromagnetic band gap," *AEU-Int. J. Electron. Commun.*, vol. 110, Oct. 2019, Art. no. 152835.
[18] A. Khan, S. Bashir, S. Ghafoor, and K. K. Qureshi, "Mutual coupling reduction using ground stub and EBG in a compact wideband MIMO-antenna," *IEEE Access*, vol. 9, pp. 40972–40979, 2021.
[19] D. Sievenpiper, L. Zhang, R. F. J. Broas, N. G. Alexopolous, and E. Yablonovitch, "High-impedance electromagnetic surfaces with a forbidden frequency band," *IEEE Trans. Microw. Theory Techn.*, vol. 47, no. 11, pp. 2059–2074, Nov. 1999.
[20] Z. Li and Y. Rahmat-Samii, "PBG, PMC and PEC ground planes: A case study of dipole antennas," in *Proc. IEEE Antennas Propag. Soc. Int. Symp., Transmitting Waves Prog. Next Millennium, Held Conjunct., USNC/URSI Nat. Radio Sci. Meeting*, Jul. 2000, pp. 674–677.
[21] Q. Zheng, C. Guo, G. A. E. Vandenbosch, and J. Ding, "Low-profile circularly polarized array with gain enhancement and RCS reduction using polarization conversion EBG structures," *IEEE Trans. Antennas Propag.*, vol. 68, no. 3, pp. 2440–2445, Mar. 2020.
[22] H. Nakano, K. Kikkawa, N. Kondo, Y. Iitsuka, and J. Yamauchi, "Low-profile equiangular spiral antenna backed by an EBG reflector," *IEEE Trans. Antennas Propag.*, vol. 57, no. 5, pp. 1309–1318, May 2009.
[23] F. Yang and Y. Rahmat-Samii, "Reflection phase characterizations of the EBG ground plane for low profile wire antenna applications," *IEEE Trans. Antennas Propag.*, vol. 51, no. 10, pp. 2691–2703, Oct. 2003.
[24] S. R. Palreddy, "Wideband electromagnetic band gap (EBG) structures, analysis and applications to antennas," Ph.D. thesis, Dept. Elect. Eng., Virginia Polytech. Inst. State Univ., Blacksburg, VA, USA, 2015.
[25] F. Yang and Y. Rahmat-Samii, "Microstrip antennas integrated with electromagnetic band-gap (EBG) structures: A low mutual coupling design for array applications," *IEEE Trans. Antennas Propag.*, vol. 51, no. 10, pp. 2936–2946, Oct. 2003.
[26] E. Rajo-Iglesias, Ó. Quevedo-Teruel, and L. Inclan-Sanchez, "Mutual coupling reduction in patch antenna arrays by using a planar EBG structure and a multilayer dielectric substrate," *IEEE Trans. Antennas Propag.*, vol. 56, no. 6, pp. 1648–1655, Jun. 2008.

[27] S. Dey, S. Dey, and S. K. Koul, "Isolation improvement of MIMO antenna using novel EBG and hair-pin shaped DGS at 5G millimeter wave band," *IEEE Access*, vol. 9, pp. 162820–162834, 2021.
[28] S. Shahparnia and O. M. Ramahi, "Simple and accurate circuit models for high-impedance surfaces embedded in printed circuit boards," in *Proc. IEEE Antennas Propag. Soc. Symp.*, Jun. 2004, pp. 3565–3568.
[29] H. Kim and R. F. Drayton, "Development of analysis method of electromagnetic bandgap (EBG) structures to predict EBG behavior based on circuit models," in *Proc. IEEE Antennas Propag. Soc. Int. Symp.*, Jul. 2006, pp. 1951–1954.
[30] M. Rahman and M. A. Stuchly, "Transmission line-periodic circuit representation of planar microwave photonic bandgap structures," *Microw. Opt. Technol. Lett.*, vol. 30, no. 1, pp. 15–19, Jul. 2001.
[31] M. Rahman and M. A. Stuchly, "Modeling and application of 2D photonic band gap structures," in *Proc. IEEE Aerosp. Conf.*, Mar. 2001, pp. 893–898.
[32] K. Brakora, C. Barth, and K. Sarabandi, "A plane-wave expansion method for analyzing propagation in 3D periodic ceramic structures," in *Proc. IEEE Antennas Propag. Soc. Int. Symp.*, Jul. 2005, pp. 192–195.
[33] S. Simsek and E. Topuz, "Some properties of generalized scattering matrix representations for metallic waveguides with periodic dielectric loading," *IEEE Trans. Microw. Theory Techn.*, vol. 55, no. 11, pp. 2336–2344, Nov. 2007.
[34] Q. Chen, F. Mesa, and O. Quevedo-Teruel, "Dispersion analysis of glide-symmetric holey metasurface based on multimodal transfer-matrix approach," in *Proc. 15th Eur. Conf. Antennas Propag. (EuCAP)*, Mar. 2021, pp. 1–4.
[35] Z. Sipus, K. Cavar, M. Bosiljevac, and E. Rajo-Iglesias, "Glide-symmetric holey structures applied to waveguide technology: Design considerations," *Sensors*, vol. 20, no. 23, p. 6871, Dec. 2020.
[36] E. Rajo-Iglesias, M. Ebrahimpouri, and O. Quevedo-Teruel, "Wideband phase shifter in groove gap waveguide technology implemented with glide-symmetric holey EBG," *IEEE Microw. Wireless Compon. Lett.*, vol. 28, no. 6, pp. 476–478, Jun. 2018.
[37] A. O. Ertay and S. Simsek, "A comprehensive auxiliary functions of generalized scattering matrix (AFGSM) method to determine bandgap characteristics of periodic structures," *AEU-Int. J. Electron. Commun.*, vol. 94, pp. 139–144, Sep. 2018.
[38] S. Simsek, "A novel method for designing one dimensional photonic crystals with given bandgap characteristics," *AEU-Int. J. Electron. Commun.*, vol. 67, no. 10, pp. 827–832, Oct. 2013.
[39] A. O. Ertay and S. Simsek, "Detection of band edge frequencies in symmetric/asymmetric dielectric loaded helix slow-wave structures," *Int. J. Circuit Theory Appl.*, vol. 50, no. 2, pp. 507–524, Feb. 2022.
[40] S. Simsek and S. A. Rezaeieh, "A design method for substrate integrated waveguide electromagnetic bandgap (SIW-EBG) filters," *AEU-Int. J. Electron. Commun.*, vol. 67, no. 11, pp. 981–983, Nov. 2013.
[41] F. Yang and Y. Rahmat-Samii, "Polarization-dependent electromagnetic band gap (PDEBG) structures: Designs and applications," *Microw. Opt. Technol. Lett.*, vol. 41, no. 6, pp. 439–444, 2004.
[42] K. Gupta, I. Bahl, and M. Bozzi, *Microstrip Lines and Slotlines*. Norwood, MA, USA: Arthech House, 1996.
[43] K. Gupta, *Microwave Solid-State Circuit Design*. New York, NY, USA: Wiley, 1988.
[44] C. A. Balanis, *Antenna Theory: Analysis and Design*. New York, NY, USA: Wiley, 2005.
[45] A. Diallo, C. Luxey, P. L. Thuc, R. Staraj, and G. Kossiavas, "Study and reduction of the mutual coupling between two mobile phone PIFAs operating in the DCS1800 and UMTS bands," *IEEE Trans. Antennas Propag.*, vol. 54, no. 11, pp. 3063–3074, Nov. 2006.
[46] R. G. Vaughan and J. B. Andersen, "Antenna diversity in mobile communications," *IEEE Trans. Veh. Technol.*, vol. VT-36, no. 4, pp. 149–172, Nov. 1987.
[47] M. Li, Y. Zhang, F. Jiang, D. Wu, K. L. Yeung, L. Jiang, and R. Murch, "Improvement for MIMO systems by increasing antenna isolation and shaping radiation pattern using hybrid network," *IEEE Trans. Ind. Electron.*, vol. 69, no. 12, pp. 13891–13901, Dec. 2022.
[48] M. Li, Y. Zhang, D. Wu, K. L. Yeung, L. Jiang, and R. Murch, "Decoupling and matching network for dual-band MIMO antennas," *IEEE Trans. Antennas Propag.*, vol. 70, no. 3, pp. 1764–1775, Mar. 2022.
[49] H.-H. Xie, Y.-C. Jiao, L.-N. Chen, and F.-S. Zhang, "An effective analysis method for EBG reducing patch antenna coupling," *Prog. Electromagn. Res. Lett.*, vol. 21, pp. 187–193, 2011.
[50] S. D. Assimonis, T. V. Yioultsis, and C. S. Antonopoulos, "Computational investigation and design of planar EBG structures for coupling reduction in antenna applications," *IEEE Trans. Magn.*, vol. 48, no. 2, pp. 771–774, Feb. 2012.
[51] L. Hu, G. Wang, J. Liang, and C. Zhang, "Novel compact mushroom-type EBG structure for electromagnetic coupling reduction of microstrip antenna array," *Frequenz*, vol. 69, nos. 3–4, pp. 89–94, Jan. 2015.
[52] O. Dahlberg, R. C. Mitchell-Thomas, and O. Quevedo-Teruel, "Reducing the dispersion of periodic structures with twist and polar glide symmetries," *Sci. Rep.*, vol. 7, no. 1, pp. 1–6, Aug. 2017.
[53] O. Quevedo-Teruel, G. Valerio, Z. Sipus, and E. Rajo-Iglesias, "Periodic structures with higher symmetries: Their applications in electromagnetic devices," *IEEE Microw. Mag.*, vol. 21, no. 11, pp. 36–49, Nov. 2020.

**DURMUS GEBESOGLU** received the B.S. degree in electronics and communication engineering from Yildiz Technical University, Istanbul, Turkey, in 2013, and the M.S. degree in electrical and electronics engineering from Middle East Technical University, Ankara, Turkey, in 2017. He is currently pursuing the Ph.D. degree in electronics and communication engineering with Istanbul Technical University (ITU), Istanbul. He has been an RF Microwave Design Engineer with Aselsan Inc., Ankara, since 2013. His current research interests include low-profile antennas and electromagnetic bandgap structures.

**AGAH OKTAY ERTAY** received the B.S. degree in electronics and communication engineering from Yildiz Technical University, Istanbul, Turkey, in 2010, and the M.S. and Ph.D. degrees in telecommunication engineering from Istanbul Technical University (ITU), Istanbul, in 2014 and 2019, respectively. He was a Research Assistant with the Department of Electronics and Communication Engineering, ITU, from 2011 to 2019. He has been an Assistant Professor with the Department of Electrical and Electronics Engineering, Erzincan Binali Yildirim University, Erzincan, Turkey, since 2019. His research interests include electromagnetic bandgap structures, microwave circuits, and slow wave structures.

**SERKAN SIMSEK** received the B.S. degree in electrical and electronics engineering from Istanbul University, Istanbul, Turkey, in 2001, and the M.S. and Ph.D. degrees in electronics and communication engineering (ECE) from Istanbul Technical University (ITU), Istanbul, in 2003 and 2008, respectively. He is currently a Full Professor with the Department of ECE, ITU. His research interests include guided wave theory, periodic structures, and photonic crystals.